Nanofluid Assisted-Chemical Oil Recovery Process at High Temperature and High Salinity Conditions: Nanofluid Stability, Interfacial Tension, Contact Angle, Microscale Experimental Investigation

Mohammad Hashemi
Petroleum University of Technology
Yousef Tamsilian (tamsilian@gmail.com)
Shahid Chamran University of Ahvaz https://orcid.org/0000-0001-6883-910X
Shahin Kord
Petroleum University of Technology

Research Article

Keywords: Nanofluid, Stability, High Temperature, High Salinity, Oil Recovery

Posted Date: July 3rd, 2023

DOI: https://doi.org/10.21203/rs.3.rs-3094697/v1

Nanofluid Assisted-Chemical Oil Recovery Process at High Temperature and High Salinity Conditions: Nanofluid Stability, Interfacial Tension, Contact Angle, Microscale Experimental Investigation

Mohammad Hashemi[a], Yousef Tamsilian[b,*], Shahin Kord[a,*]

[a] Department of Petroleum Engineering, Ahvaz Faculty of Petroleum, Petroleum University of Technology, Ahvaz, Iran, hashemi3773@gmail.com, sh.kord@put.ac.ir

[b] Department of Chemical Engineering, Faculty of Engineering, Shahid Chamran University of Ahvaz, Ahvaz, Iran, tamsilian@scu.ac.ir

ABSTRACT

One of the most important aspects to use the nanofluid flow through the oil recovery process is physical and chemical constraints at high salinity and temperature, harsh conditions, leading to the instability and further problems. In this study, the stability of various nanoparticles, Al_2O_3, SiO_2, ZrO_2, TiO_2, Fe_2O_3, nanoclay, and ZnO, were examined upon the concentration (0.01 to 3 wt%), temperature (ambient and 75°C), salinity (20,000 to 80,000 ppm), pH (2 to 12), and stabilizers of polyethylene glycol, polyvinylpyrrolidone, guar gum, Triton X-100, sodium dodecyl sulfate, cetrimonium bromide. Then, the most stable nanofluid was nominated to investigate the oil recovery mechanisms by performing interfacial tension (IFT), wettability alteration, and micromodel flooding analyses. Zinc oxide and silicon dioxide nanofluids were maintained their stability at the harsh conditions and guar gum showed a good performance in stabilizing nanofluids, compared to other nanofluids agglomerated. According to the results of the IFT reduction upon the nanofluid and reservoir crude oil (1.64 mN/m), wettability alteration of carbonate cores (113.68 degree) and micromodel experiments (additional recovery of 32.23% and 6.27% in the secondary and tertiary flooding, respectively) all compared to the seawater, the ZnO nanofluid stabilized by guar gum was an excellent candidate to use in the oil recovery projects.

KEYWORDS: Nanofluid, Stability, High Temperature, High Salinity, Oil Recovery

INTRODUCTION

Getting more hydrocarbons out of the underground reservoirs is economically facilitated by reducing the residual oil saturation, turning multiphase into single-phase flow/maintaining a single-phase situation during the pushing injection, reducing interfacial tension, wettability alteration of oil-wet to water-wet surfaces. On the other hand, nanoparticles (NPs) have been extensively used in different industries including biomedical, electronics, materials, pharmaceutical, aerospace, manufacturing, photography, and more recently the energy sectors. Totally, there are three positive aspects for NPs to use in the industrial sectors: first they can be modified in size and shape. Second, chemical properties of the NP surface can be altered to either hydrophilic or hydrophobic. Last, most of NPs are assumed as environmentally friendly agents [1]. Because of the magnificent properties, nanoparticles, as one of the most used nanostructures, gained too much attention in the oil and gas industries, specifically in improved (IOR) and enhanced oil recovery (EOR) operations [2]. Refer to the nanoparticles' size and altering their surface characteristics to manipulate special optical, interfacial, magnetic, chemical or electrical features for making them more promising for operational utilizations, NPs flooding may alter the interfacial tension (IFT) and surface wettability through the porous media [3]. Aluminum oxide, magnesium oxide, zirconium dioxide, cerium(IV) oxide, titanium dioxide, zinc oxide and iron(III) oxide have the most widely utilized, exhibiting the excellent chemical and physical characteristics in various applications [4]. Some recent works on the nanostructure-assisted chemical oil recovery processes were tabulated in **Table 1**.

Table 1. Recent works on nanostructure-assisted chemical oil recovery processes

Researchers	Subject	Materials	Main Observations	Year, References
Haroun et al.	Investigating oil recovery	CuO, Fe_2O_3, NiO_2 nanofluids	Averagely 14% increasing in recovery	2012, [5]
Li et al.	Applying hydrophilic nano-SiO_2 through oil recovery	Nano-SiO_2 in the presence of 30,000 ppm NaCl solution with 0.05 wt% NPs	Lowering interfacial tension and altering wettability of sandstone reservoirs at an optimum concentration	2013, [6]
Esfandyari Bayat et al.	Studying interfacial tension and viscosity of injected fluid	Al_2O_3 and ZnO NPs in the presence of sodium dodecyl sulfate surfactant (SDS) alongside pure SDS fluid	Increasing viscosity and decreasing interfacial tension of nanofluids compared to SDS surfactant fluid	2014, [7]
Hendraningrat et al.	Investigating three hydrophilic NPs through EOR of various wettability sandstone reservoirs	Al_2O_3, TiO_2 and SiO_2	Observing IFT reduction as one of contributing mechanisms in aforementioned NPs	2015, [8]
Lee et al.	Using sol-gel method	Synthesized ZnO NPs in three sizes of 41-45, 66-70, and 86-90 nm	Increasing viscosity and surface tension by NP size	2016, [9]
Yousefvand et al.	Analyzing effect of SiO_2 NPs addition on NaCl/HPAM/SDS solution performance in a micromodel	SiO_2 NPs, NaCl, HPAM, SDS	Altering rock wettability towards more water-wetness	2018, [10]
Rezk et al.	Investigating recovery factor in tertiary injection process	ZnO/SDS nanofluid and SDS surfactant solutions	Obtaining higher recovery factor in tertiary injection process in core flood system at optimum concentration of 0.05 wt%	2019, [11]
Mahpishanian et al.	Experimental investigation of nano-SiO_2 on wettability alteration and enhanced oil recovery from carbonate reservoir Using low salinity water	SiO_2	Increasing 11.71% RF of spontaneous imbibition process by 0.05 wt% silica NP in diluted see water (1000 ppm) compare to diluted see water (1000 ppm) at	2020, [12]
Rashidi et al.	Performance of environmentally friendly water-based calcium carbonate nanofluid as enhanced recovery agent for sandstone oil reservoirs	$CaCO_3$	Resulted in 20% additional recovery by flooding 0.025 wt% calcium carbonate nanofluid into oil-wet 2-D glass micromodel compared to normal water flooding	2021, [13]
Bila & Torsæter	Experimental Investigation of polymer-coated silica nanoparticles for EOR under harsh reservoir conditions of high temperature and salinity	SiO_2, Al_2O_3 & MOX (SiO_2 > 98.3%)	Increasing oil recovery after core flooding (up to 6% of OOIP)	2021, [14]
Keykhosravi et al.	TiO_2 nanoparticle-induced xanthan gum polymer for EOR: Assessing the underlying mechanisms in oil-wet carbonates	Anatase TiO_2 & Xanthan gum	25% extra oil of OOIP recovered using Nano-polymer suspension	2021, [15]
Gu et al.	Microscopic mechanical model analysis and visualization investigation of SiO_2	Sodium dodecyl sulfate (SDS) surfactant and foam prepared by a combination of partially	Polymer and nanoparticles amplified force between foam liquid film and heavy oil by	2022, [16]

Researchers	Subject	Materials	Main Observations	Year, References
	nanoparticle/HPAM polymer foam liquid film displacing heavy oil	hydrolyzed polyacrylamide (HPAM) polymer and SiO_2 nanoparticles	1.95 and 2.2 times, and oil recovery efficiency increased from 42.43 to 57.82%	
Xu et al.	Extensional rheology of hydrophobically associating polyacrylamide solution used in chemical flooding	HAHPAM solution, NaCl, surfactant	By increasing concentration and decreasing temperature, filament breakup time and extensional viscosity of HAHPAM solution increase, NaCl delaying HAHPAM filament attenuation by increasing solution extensional viscosity and surface tension, filament stability of HAHPAM/SDS solution in presence of sodium dodecyl sulfate (SDS)	2023, [17]
Pu et al.	Facile synthesis of chromium chloride/poly(methyl methacrylate) core/shell nanocapsules and application as delayed crosslinker in secondary oil recovery	Chromium chloride/poly(methyl methacrylate) (PMMA) nanocapsules, HPAM	exhibiting the tunable size (358–983 nm), Cr loading (7.1%–19.1%), and Cr entrapment efficiency (11.7%–80.2%), Cr(III) release delay of and prolonging gelation time of HPAM up to 27 days.	2023, [18]

According to the previous works, many NPs have been utilized in the IOR and EOR processes, including SiO_2, Al_2O_3, TiO_2 ZrO_2, Fe_2O_3, ZnO and nanoclay NPs being more scrutinized and exhibiting an excellent performance through the oil recovery. However, fewer experiments were performed in terms of both economically and reservoir performance. A considerable gap in the previous works seems to be the nanofluid limitation at the high salinity and temperature values leading to their agglomeration and instability. Due to the fact that most of the world's reservoirs (for example Iranian oil reservoirs) exhibit high salinity and temperature, hence, unravelling the challenges associated with these two parameters has received much importance in the stable nanofluid injection through the EOR processes. For this reason, introducing a nanofluid that shows a good stability at harsh conditions of high salinity and temperature has become a significant issue up to now.

The synergic effects existing between the surfactant/polymer and NPs on main oil recovery mechanisms, including water phase viscosifying, IFT reduction, wettability alteration (towards more water-wetness), and oil viscosity lowering, are considered more favorable compared to the cases which the individual chemicals were utilized [19]. In addition, the surfactants in a nanofluid solution might lead to the high stability provision for the NPs. Regarding the promising effects of synergism between NPs and surfactants, utilizing stable surfactants was assumed at high salinity and high temperature conditions to stabilize the NPs in a suspension as a highly-recommended approach [20].

Efficient surfactants and polymers being utilized in the literatures can be summarized as sodium dodecyl sulfate (SDS) [10, 21-30], sodium dodecyl benzene sulfonate (SDBS) [31-39], cetyl trimethyl ammonium bromide (CTAB) [40-46], dodecyl trimethyl ammonium bromide (DTAB) and sodium octanoate (SOCT) [40, 47], hexadecyl trimethyl ammonium bromide (HCTAB), polyvinyl pyrrolidone (PVP), polyethylene glycol (PEG) [48-52], Arabian gum [53, 54] and guar gum [55, 56]. The appropriate selection of surfactants is regarded as the most significant part of the surfactant-assisted chemical EOR procedure. The utilized surfactant might be anionic, cationic or nonionic [57]. However, the addition of surfactants and polymers may bring some disadvantages at high temperatures [58, 59]. In temperatures more than 60 °C, the bonding between NPs and surfactant can be damaged, and hence, the nanofluid loses its stability and NPs start to precipitate [43, 46, 60, 61].

In 2016, Hendraningrat et al. analyzed the stability of nanofluid of Al_2O_3, TiO_2 and SiO_2 NPs through the visual stability, particle size, and conductivity measurements [9]. Through the

visual analysis, it was perceived that Al_2O_3 NPs tended to precipitate at initial stages (nearly after 3 hours) while TiO_2 NPs precipitated slightly later. However, a better stability was exhibited by SiO_2 NPs after 24-48 hours. The results of visual stabilities were in accordance to the particle size measurements in a way that the average size of Al_2O_3 NPs enlarged six times, demonstrating the maximum limit of agglomeration.

One of the most significant factors which is strongly pertinent to the NPs stability in a suspension is zeta potential concept [62]. In a nanofluid suspension, each particle has a surface charge being encompassed with a hydrodynamic diameter. The surface charge and stability of nanofluids are affected by the pH value of the nanofluid solution. Based on the Hendraningrat et al.'s investigation, there was an optimal pH value in which the highest nanofluid stability was achieved [8].

Based on Yousefvand et al.'s observations, considering a system of NaCl/HPAM/SDS solution plus SiO_2 NPs, the existence of salt was the major factor of nanosilica instability and both monovalent and divalent ions acted similarly at the high salt concentrations. Last but not the least, at NaCl concentrations less than 30,000 ppm, SDS acted as a stabilizer and was capable to compensate the NaCl detrimental impacts through being adsorbed on the NP surfaces and reinforcing the repulsion forces which existed between nanosilica particles [10].

In 2016, Adil et al. investigated ZnO nanofluids as well as SDS and SDBS stabilizers at 95 °C. The base fluid used by Adil et al. contained 30,000 ppm NaCl salt. It was concluded that the most stable aqueous dispersion of ZnO NPs was at 0.1 wt% concentration, utilizing 0.025 wt% sodium dodecyl benzene sulfonate. This was due to the fact that the formation of micelles on the NP-bound surfactants caused the enhancement in repulsive forces which consequently increased the nanofluid stability [63].

In 2018, Nourafkan et al. suggested a new strategy for synthesizing iron oxide NPs to provide a longer stability. The synthesis was done in a brine solution and a mixture of internal olefin sulfonate (IOS) anionic surfactant with a high thermal stability and alkyl alkoxy sulfate (AAS) anionic surfactant & ethoxylated alcohol (EA) nonionic surfactant with a high salinity stability. It was observed that a mixture of IOS anionic surfactant and EA nonionic surfactant resulted in a desirable stability for iron oxide NPs. Finding an optimized synergic effect led to the provision of the most stable nanofluid [64].

Up to the best knowledge of the authors, the nanofluid restrictions at high salinity and temperature values leading to agglomeration and instability have not been comprehensively investigated for using in the oil recovery. In the event that most of the world's hydrocarbon reservoirs, like Iranian ones, have been produced at such harsh conditions, hence, unravelling has received much importance in stable nanofluid injection through EOR processes. For this reason, a comprehensive studying the challenges associated with these two parameters and introducing a nanofluid to show a good stability at high salinity and temperature has become a significant issue. Hence the purposes of this study were the investigation of the stability of various nanoparticles, aluminum oxide, silicon dioxide, zirconium dioxide, titanium oxide, Iron(III) oxide, nanoclay, and zinc oxide, as function of the nanoparticle concentration (0.01 to 3 wt%), temperature (ambient to 75 °C), salinity (20,000, 80,000 ppm), pH (2 to 12), and stabilizer of polyethylene glycol (PEG), polyvinylpyrrolidone (PVP), guar gum, Triton X-100 (TX-100), sodium dodecyl sulfate (SDS), cetrimonium bromide (CTAB). Then, the analyses of interfacial tension (IFT), wettability alteration, and micromodel flooding were

experimentally performed for the most stable nanofluid at high temperature and salinity conditions. These goals ultimately led to the introduction of nanofluids that had good stability for more than one month at high temperatures and salinity (salinity 80,000 ppm and 75 °C) and also had a good potential for the oil recovery process by measuring the rate of changing in wettability, interfacial tension and injection into the micromodel.

EXPERIMENTAL DESIGN AND PROCEDURE

Materials

The specification of aluminum oxide (Al_2O_3), silicon dioxide (SiO_2), zirconium dioxide (ZrO_2), titanium oxide (TiO_2), Iron(III) oxide (Fe_2O_3), and zinc oxide (ZnO) nanoparticles provided by US Research Nanomaterials and nanoclay particles provided by Sigma-Aldrich, are illustrated in **Table 2**. All NPs were hydrophilic and in powder form. A variety of stabilizers including polymers (guar gum, PEG, and PVP), anionic (SDS), cationic (CTAB) and nonionic (TX-100) surfactants were prepared by Merck Company (Germany), presented in **Table 3**. The crude oil sample and carbonate thin slices were collected from one of the southern Iranian oilfields. The polarity of the crude oil (e.g., asphaltene and resins) was due to the heteroatoms such as sulfur, nitrogen, and oxygen existing in the functional groups of acidic and basic organic molecules. Using a filtration paper with an average pore diameter of 5 mm in addition to a vacuum pump, allowed solid particles to be removed from the sample. The chemical specification analysis of the sample is listed in **Table 4**. The viscosity, density, and asphaltene content were measured using Cannon Fenske viscometer (size=200, Cannon Instrument Company, USA), DMA45 digital densitometer (Anton Paar, Austria), and modified method of standard IP143 method [54], respectively.

The salts of NaCl, KCl, $CaCl_2$, $MgCl_2$ ($6H_2O$), Na_2SO_4 and $NaHCO_3$ dissolved in deionized water were purchased from Merck Company (Germany) with the purity of 99%. They were used to prepare synthetic seawater (according to Persian Gulf seawater components and total dissolved salinity (TDS) of 40,572 ppm) and different diluted formation water (based on the formation water of the southern Iranian oilfield). Ion concentrations in brine solutions are brought in **Table 5**.

Table 2. Nanoparticle properties used in this study

Nanoparticle	Purity (%)	Chemical Formula	Color	Morphology	Specific Surface Area (m^2/g)	Average Particle Size (nm)	True Density (g/cm^3)
Aluminum Oxide - Alpha	+99	Al_2O_3	White	Nearly Spherical	>19	50	3.97
Silicon Dioxide	+99	SiO_2	White	Amorphous	180-600	20-30	2.40
Zirconium Dioxide	99.95	ZrO_2	White	Nearly Spherical	30-60	20	5.89
Titanium Oxide -Rutile	+99.9	TiO_2	White	Spherical	35-60	30	4.23
Iron(III) Oxide - Alpha	+98	Fe_2O_3	Red Brown	Spherical	40-60	20-40	5.24
Nanoclay Montmorillonite	+99	N/A	Pale Yellow	Nearly Spherical	20-60	1-2	0.70
Zinc Oxide	+99	ZnO	White	Nearly Spherical	20-60	10-30	5.61

Table 3. Stabilizer properties used in this study

Type	Name	Average density @20 °C (g/cm^3)	Molar Mass (g/mol)	pH value	Chemical Formula
Polymers	**PEG**	1.2	5400	5-7	$HO(C_2H_4O)nH$
	PVP	1.2	---	3-5	$(C_6H_9NO)n$
	Guar gum	0.8-1.0	--	5-7	$C_{10}H_{14}N_5Na_2O_{12}P_3$
Surfactants	**TX-100, Nonionic**	---	647	---	$C_{14}H_{22}O(C_2H_4O)n$
	SDS, Anionic	1.03	288.37	6-9	$C_{12}H_{25}NaO_4S$
	CTAB, Cationic	---	364.46	---	$C_{19}H_{42}BrN$

Table 4. Crude oil properties used in this study

Properties	Value	Unit
Density at 24 °C	0.93	gr/mL
API	20.65	degree
Acid number	2.9	mg KOH/g oil
Saturates	50.12	wt%
Aromatics	34.97	wt%
Resins	7.01	wt%
Asphaltene	7.9	wt%
Viscosity at 25 °C	41.16	cp

Table 5. Ion concentrations in brine solutions used in this study

Type	Na^+ (ppm)	K^+ (ppm)	Mg^{2+} (ppm)	Ca^{2+} (ppm)	Cl^- (ppm)	HCO_3^- (ppm)	SO_4^{2-} (ppm)	TDS (ppm)
FW	66,620	101	1312	3820	111,026	288	1,633	184,800
SW	12,290	280	1530	460	22,652	150	3,210	40,572
FW2	7,210	11	142	413	12,016	31	177	20,000
FW8	28,840	44	568	1,654	48,063	125	706	80,000

Methodology

The nanofluid consisted of two parts, the base fluid and nanoparticles suspended therein. Deionized water, seawater, formation water, diluted formation and seawater are used as base fluid. To make the brine, the required salts in the **Table 5** were added one by one into the deionized water and then stirred with magnetic stirrer (Labinco L81, Netherland). After introducing each salt, the fluid was allowed to be completely homogenized. Then, the considered nanoparticle was added. In case of the nanofluid stabilized by a polymer or surfactant, after 10 minutes, the stabilizer was introduced to the final solution and stirred for 30 minutes. Then, by adding HCl and NaOH, the acidity and basicity value of each nanofluid were adjusted. Next, the prepared solution was dispersed for an hour in an ultrasonic bath (VCLEAN1-L02, Iran).

To investigate the nanofluids behavior during the oil recovery process, the essential tests including characterization, stability tests, contact angle, interfacial tension, micromodel flooding were implemented. Scanning electron microscope (SEM) and transmission electron microscope (TEM) tests were obtained from the chemical provider to survey the as-prepared nanostructures and samples. Additionally, dynamic light scattering (DLS) and visual tests were conducted to analyze the nanofluids stability and the most stable nanofluids were chosen for the following analyses. Ultimately, a couple of contact angle and interfacial tension measurements as well as glass micromodel flooding tests were conducted to microscopically assess the NPs behaviors at the pore scale. **Figure 1** shows the roadmap of this work to study the nanofluid assisted-chemical oil recovery process.

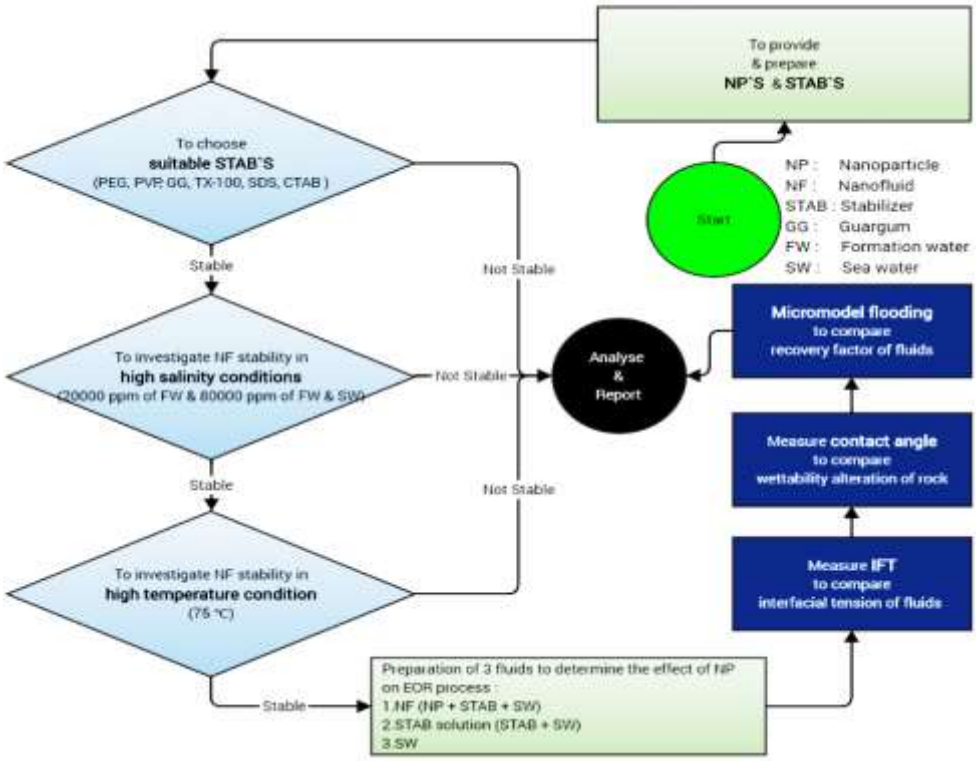

Figure 1. Roadmap of this work to study nanofluid assisted-chemical oil recovery process

Characterization

TEM and SEM images taken from the chemical provider are presented in **Figure 2** and **3**. The nanofluid dispersion was investigated by dynamic light scattering (DLS, Malvern ZEN3600, UK) in different time after the sonication.

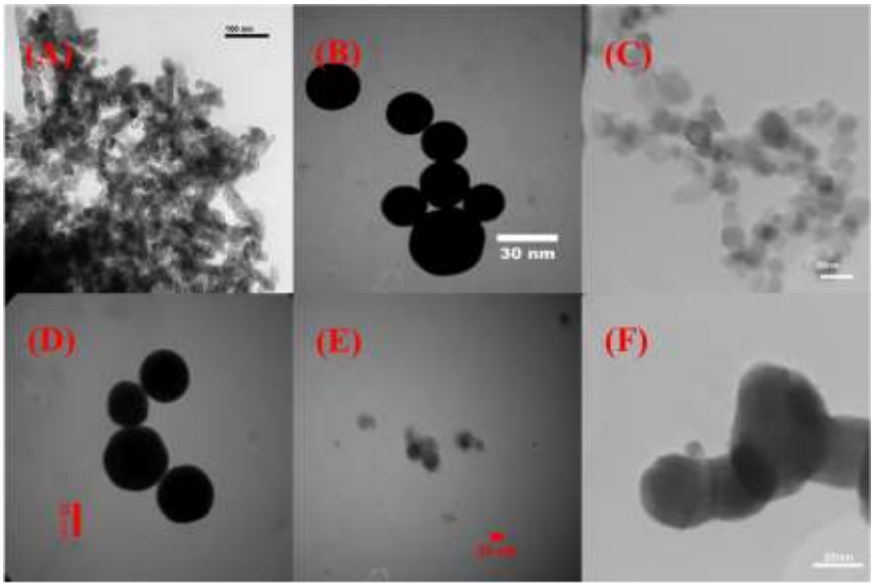

Figure 2. TEM results of nanoparticles: (A) SiO_2, (B): TiO_2, (C) Al_2O_3, (D) Fe_2O_3, (E) ZrO_2, (F) ZnO

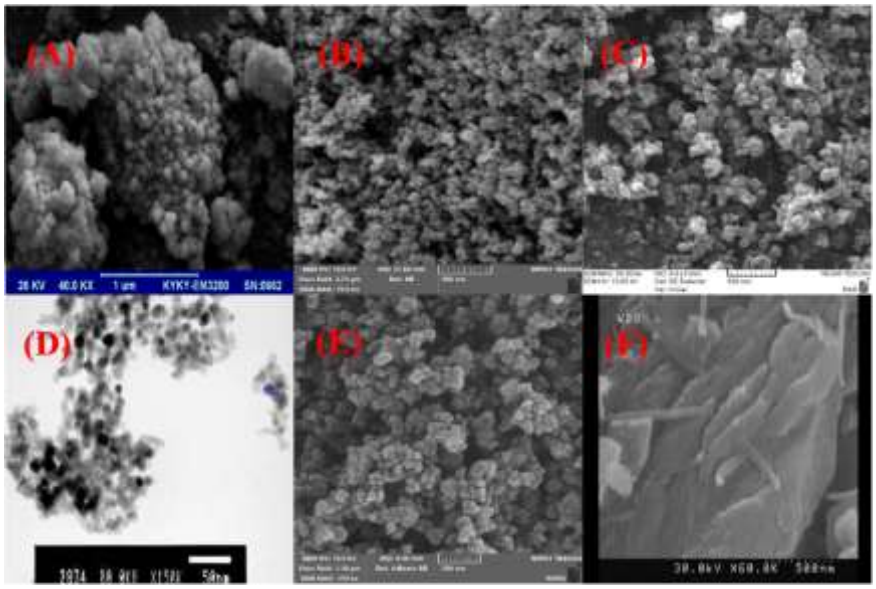

Figure 3. SEM results of nanoparticles: (A) TiO_2, (B) Al_2O_3, (C) Fe_2O_3, (D) ZrO_2, (E) ZnO, (F) Nanoclay

Nanofluid Stability Tests

To evaluate the stability of nanofluids, after preparation, each nanofluid was checked by visually imaging. Then, the selected nanofluids exhibiting a good stability were tested by DLS identifier (Malvern ZEN3600, UK) to study the quality of its stability. **Table 6** shows the nanofluid stability assessment procedures. A Canon camera (EOS 70, Japan) was used to record the required photos.

Table 6. Nanofluid stability assessment procedure

Step	Description
1	To evaluate the stability of silica NPs with different concentrations (0.01, 0.05, 0.1, 0.3, 0.5 and 3 wt%) in deionized water-based fluid and then determine the optimum concentration for the further stability,
2	To investigate the stability of other NPs at the optimum concentration of Step 1 in deionized water,
3	To select the most stable and unstable nanofluids in Step 2, then examine, test and select the appropriate stabilizers upon the two mentioned nanofluids,
4	To evaluate stability other nanofluids with selected stabilizers in Step 3,
5	To investigate the salinity effect on the nanofluids with the selected stabilizer in Step 4 on the diluted formation water-based fluid at 20,000 ppm (FW2) salinity to screen the low stable nanofluids over the salinity,
6	To investigate the effect of increasing salinity on the highest stable nanofluids in Step 5 with the diluted formation water-based fluid at salinity of 80,000 ppm (FW8), also, to investigate the effect of pH on the stability of nanofluids and PZC point range of each NP, prepared in two acidic (1.7-2) and basic (11.7-12) condition,
7	To adjust the pH of the seawater-based nanofluids to neutral pH as long as the nanofluids keeping their stability,
8	To investigate the effect of temperature on the stability of selected nanofluids.

Interfacial Tension Measurement

Briefly, to measure the IFT, a syringe pump was fitted with a U-shape needle and filled with crude oil. Then, the syringe (SP102 HSM, Fanavaran Nano-Meghyas, Iran) was placed in a motor driven piston and the tip of the U-shaped needle was positioned in an optically clear vessel immersed in the aqueous phase. Subsequently, the crude oil droplet was positioned at the tip of the needle (22G- 0.7 mm inner diameter) and later, the drop image was recorded using a Dino-Lite Edge digital microscope camera equipped with 200X zoom (AM413ZT, Taiwan).

Contact Angle Measurement

In this study, all contact angle measurements were provided using the pendant drop method at ambient temperature and atmospheric pressure. According to this method, a drop of oil fluid was left in the aqueous fluid on a solid surface, and the contact angle was measured after a sufficient time for the equilibrium. Similar to the IFT measurement setup, the Dino-Lite Edge digital microscope camera was used for photographing and filming the drop shape. Through the contact angle measurements, seawater and nanofluid were employed as the encompassing fluids. Initially the contact angles were reported; then after one week they were checked to measure the influence of exhibition time on the wettability alteration.

Micromodel Flooding Tests

The developed micromodel was consisted of two glass plates with 6 mm thickness, 139.18 mm in length, and 60.59 mm in width designed by a well-known and high accuracy software. Due to the challenges of non-repeatability results of the most micromodel patterns, it was decided to utilize the homogeneous double permeability pattern illustrated in **Figure 4A**. To investigate the nanofluids effect upon the interfacial tension inside the micromodel and the behavior of nanofluids and their impact on trapped oils in dead-end pores, the pores are designed in triangular, as depicted in **Figure 4B**.

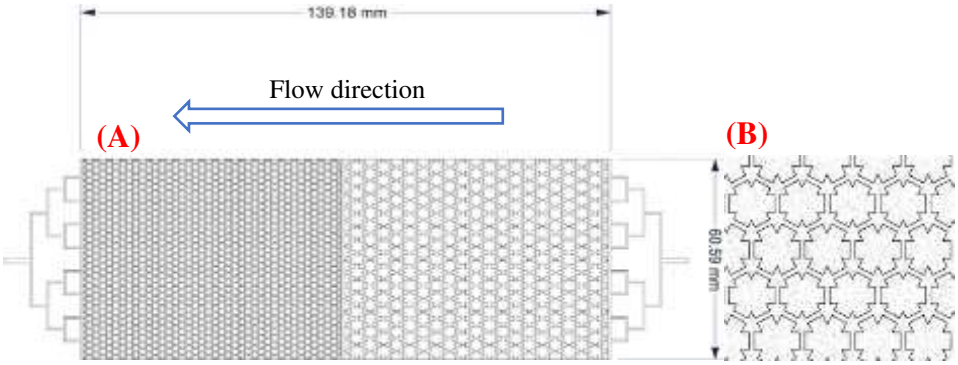

Figure 4. (A) Micromodel pattern and size and (B) illustration of triangular-shaped holes included in glass micromodel

All physical and hydraulic specification of the used micromodel determined by photo analysis and laboratory measurements are mentioned in **Table 7**.

Table 7. Specification of glass micromodel used in this study

Parameters	Value	Unit
Pore Volume (PV)	0.445	cm^3
Average Depth (D)	143	µm
Permeability (K)	455	mD
Porosity (Ø)	36.86	%
Width (W)	60.59	mm
Length (L)	139.18	mm
Pore throat in high permeable zone	330	µm
Pore size in High permeable zone	1.35	mm
Pore throat in low permeable zone	160	µm
Pore size in low permeable zone	0.7	mm

Four experiments were implemented on this micromodel, including secondary injection of seawater (2PV), secondary injection of seawater-based stabilizer solution (0.05 wt%, 2PV), secondary injection of seawater-based stabilized nanofluid (the optimum concentration, 2PV) and tertiary injection of nanofluid, initially seawater injection up to 2 PV and then injecting 2 PV of seawater-based zinc oxide nanofluid. All these tests were conducted in ambient conditions. The cleaning process was achieved by flushing solvent through the micromodel prior to starting each test. Three cleaning fluids in subsequent of toluene, acetone, and distilled water were used for the washing procedure. The injection rate for the oil and water was set as a constant flow rate of 0.1 mL/h. Each test was conducted in a 9-hour time duration. The utilized micromodel setup comprised of an equipped camera to capture high resolution pictures, a precise differential pressure gauge (DP) for measuring pressure and absolute permeability calculation, a highly accurate syringe pump for controlling the fluids flow through the micromodel medium and finally a light source to enhance the visualization.

The fluid injection was initiated from the high permeable side of micromodel. The displacement procedure was commenced by fluids injection through the model at a constant rate without any water pre-flush. In order to create an oil-wet condition for glass micromodel before conducting each test, the micromodel was saturated with oil for 48 hours. Prior to each flooding test, the glass micromodel was cleaned with injecting toluene, and then with flushing acetone and distilled water. During each test, the micromodel was photographed, so the image-processing techniques were utilized to calculate the oil recovery factor through the displacement process. During the flooding experiments, all models were placed horizontally in ambient conditions and the oil and the aqueous solution were in black and white hues, respectively. The haphazard oil-wet distribution in matrix was resulted from the various form of the matrix surface shape during the etching process. Therefore, a random distribution of aging process was observed through the micromodel.

RESULTS AND DISCUSSION

Stability of Nanofluids

Refer to **Table 6**, firstly, the stability of silica NPs with a concentration of 0.01 to 3 wt% in deionized water-based fluid was investigated. **Figure 5A** shows the stability of SiO_2 nanofluid with different concentrations after one month. Hence, as the NP concentration increased, the stability of the nanofluid decreased. Considering the sediment amount in this figure as well as the experiments done by Hendraningrat et al. [9] and Rezk et al. [11], a concentration of 0.05 wt% could be considered as an optimal concentration to the following experiments.

The second step involved was to investigate the stability of various other nanostructures (TiO_2, Fe_2O_3, ZnO, ZrO_2, nanoclay, and Al_2O_3) at the concentration of 0.05 wt% in deionized water. **Figure 5B to G** give the relevant data for 60 minutes after the preparation of each nanofluid. All nanofluids were completely homogeneous and dispersed immediately after the ultrasonic dispersion, and no NP's sediment was observed at the bottom of the container. 60 minutes after the sonication, as can be seen, the lowest and highest NPs depositions were related to aluminum oxide and titanium oxide, respectively. As a result, the most stable and unstable NPs in deionized water were selected for the further experiments.

In the third step, aluminum oxide and titanium dioxide were dispersed in the deionized water-based fluid by the stabilizers presented in **Figure 6**. These figures show the sediment of nanofluids with stabilizers one hour after the sonication for the mixture of 0.05 wt% NPs and

0.05 wt% stabilizer in deionized water. By comparing the stabilizer performance, guar gum polymer performed very well and left less sediment in nanofluid (**Figure 6F, G**). In fourth step, the stability of other nanofluids, Fe_2O_3, ZnO, ZrO_2, nanoclay, at concentration of 0.05 wt% was also investigated by guar gum polymer in concentration of 0.05 wt%. It was observed that the nanofluids maintained their stability for a much longer time than that of the non-polymer state; hence, infinitesimal deposits were formed. Subsequently, it can be concluded that guar gum polymer was a desirable candidate to generally increase the stability of nanofluids for the next steps.

The fifth step was to investigate the salinity effect on the stability of nanofluids in 20,000 ppm diluted formation water (FW2). All NPs (0.05 wt%) were dispersed along with guar gum polymer (0.05 wt%) in FW2 base fluid. Examining the stability of the nanofluids, Fe_2O_3 and Al_2O_3 left a considerable amount of deposition in less than 30 minutes (**Figure 7A**). According to the results of the stability study, these two nanofluids were not resistant to the salinity, because of probably formation of salt bridges among NPs [65]. Saleh et al. [66] and He et al. [67] found that the stability of NPs in aqueous phases was proportional to the amount of ionic strength (salt), where higher ionic strength led to the higher NP suspension instability. Against, **Figure 7B** shows the acceptable stability of other nanofluids in the salinity of 20,000 ppm one hour after the sonication.

In the sixth step, the stability of the remaining nanofluids except Al_2O_3 and Fe_2O_3 was tested with higher salinity (80,000 ppm diluted formation water, FW8). Also, to investigate the effect of pH parameter on the stability of nanofluids and the PZC point range of each NP, nanofluids were prepared in two acidic (1.7-2) and basic (11.7-12) pH values. The reason for choosing these pH ranges was to ensure that the pH of all nanofluids in the acidic medium was lower than PZC and in the alkaline medium was higher than PZC, having the same surface charge of the NPs in the nanofluids. Among all the nanofluids in this step, only ZnO and SiO_2 remained stable in the acidic media. Rest of the nanofluids, on average, showed a significant deposition after one day (**Figure 8A,B**). According to the results of this step, the acidic environment caused the nanofluids to be more stable than the basic one; hence, preventing the NPs from the agglomeration. As mentioned earlier, since each nanoparticle has a PZC, the stability of the solution can be changed by decreasing or increasing the acidity of the solution. Thus, the configuration of interactions on an interface is different according to relative magnitude of acidity/basicity between the particle and solvent. If there is no or less difference in acidity/basicity between the particle surface and solvent, the particle would not be charged [68]. Given the PZCs of nanoparticles used in this experiment in the range of $6.6<pH<11$, the acidic environment (pH=1.7-2) made more stability than the alkaline environment (pH=11.7-12) because of a higher pH difference.

In the seventh step, due to the reduction of huge injection expenditures in the realistic conditions, seawater was utilized as the base fluid. By increasing the pH until the nanofluid remained stable and desirable for the injection process in the reservoir, the stability of the nanofluid was investigated. ZnO and SiO_2 nanofluids maintained their stability up to pH=5, higher pH values caused to agglomerate the NPs and deposit up to one hour after sonication.

In the last step, the temperature effect on the ZnO and SiO_2 nanofluids containing NPs (0.05 wt%), guar gum (0.05 wt%), and seawater (40,572 ppm) was investigated. Thus, the ZnO and SiO_2 nanofluids were exposed to 75 °C for one month. In addition to these two nanofluids,

SiO_2/ZnO hybrids were also tested under the same temperature, salinity and pH value. **Figure 8C** shows the stability of the mentioned nanofluids immediately after sonication, after one day, one week and also one month. As can be seen, silica nanofluid and silica/zinc oxide hybrids lost their stability and deposited under the high temperature and salinity. However, zinc oxide nanofluid still retained its stability even after a month. The positive effect of increasing temperature on the ZnO nanofluid was agreed with the obtained results by Adil et al. where ZnO nanoparticles stabilized with SDBS oleic acid and SDS [64].

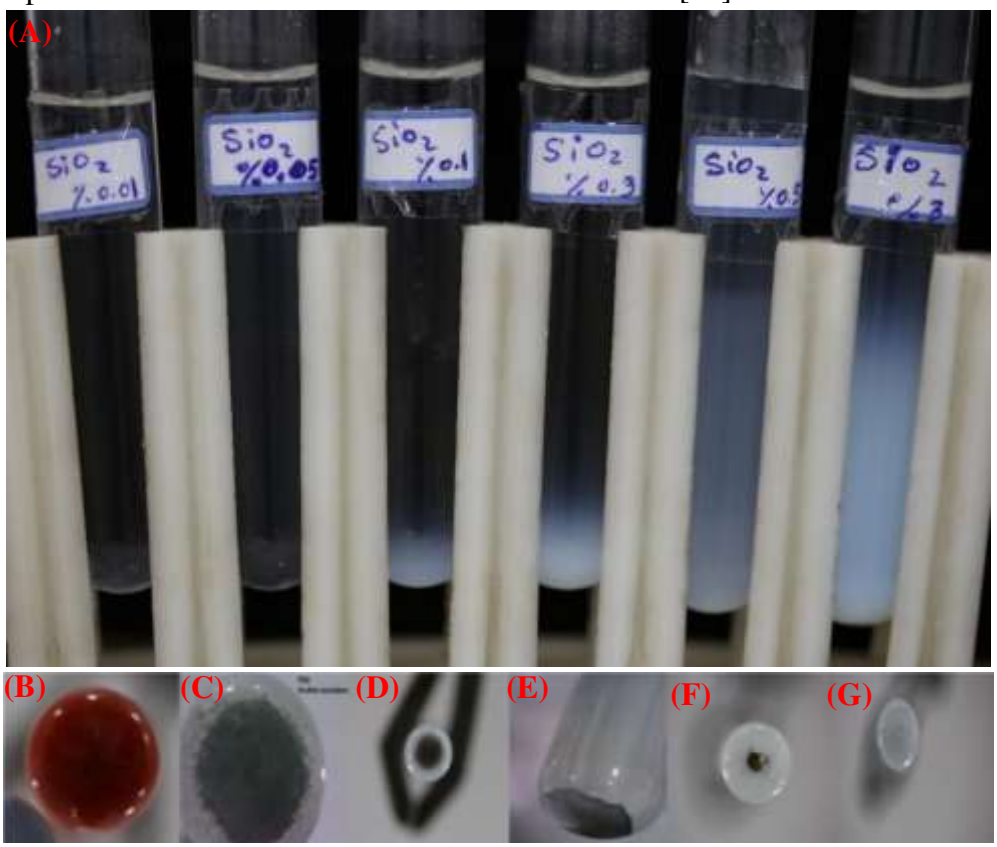

Figure 5. Visual stability of (A) SiO_2 in different concentrations, (B) Fe_2O_3, (C) TiO_2, (D) ZnO, (E) ZrO_2, (F) nanoclay, and (G) Al_2O_3 at 0.05 wt% in deionized water after one month

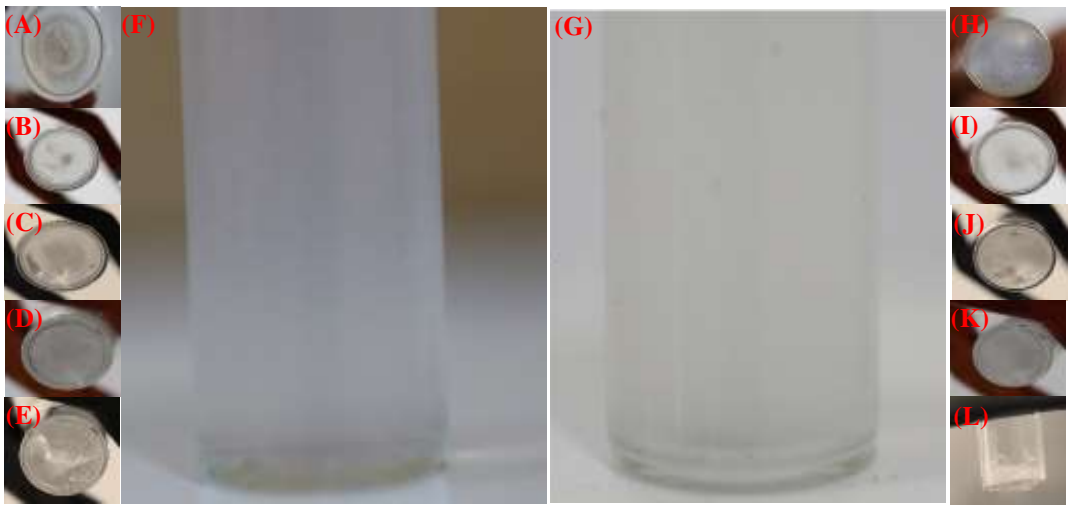

Figure 6. Evaluation of different stabilizers (A, H) PEG, (B, I) PVP, (C, J) TX100, (D, K) SDS, (E, L) CTAB, (F, G) guar gum on Al_2O_3 and TiO_2 nanofluids stability, respectively (NP: 0.05 wt%, stabilizer: 0.05 wt%, deionized water)

Figure 7. (A) Significant precipitation of Al_2O_3 and Fe_2O_3 nanofluid after 30 min, (B) SiO_2, TiO_2, ZrO_2, ZnO_2 and nanoclay nanofluid after one hour (base fluid: 20,000 ppm diluted formation water, FW2, NP: 0.05 wt%, guar gum polymer: 0.05 wt%)

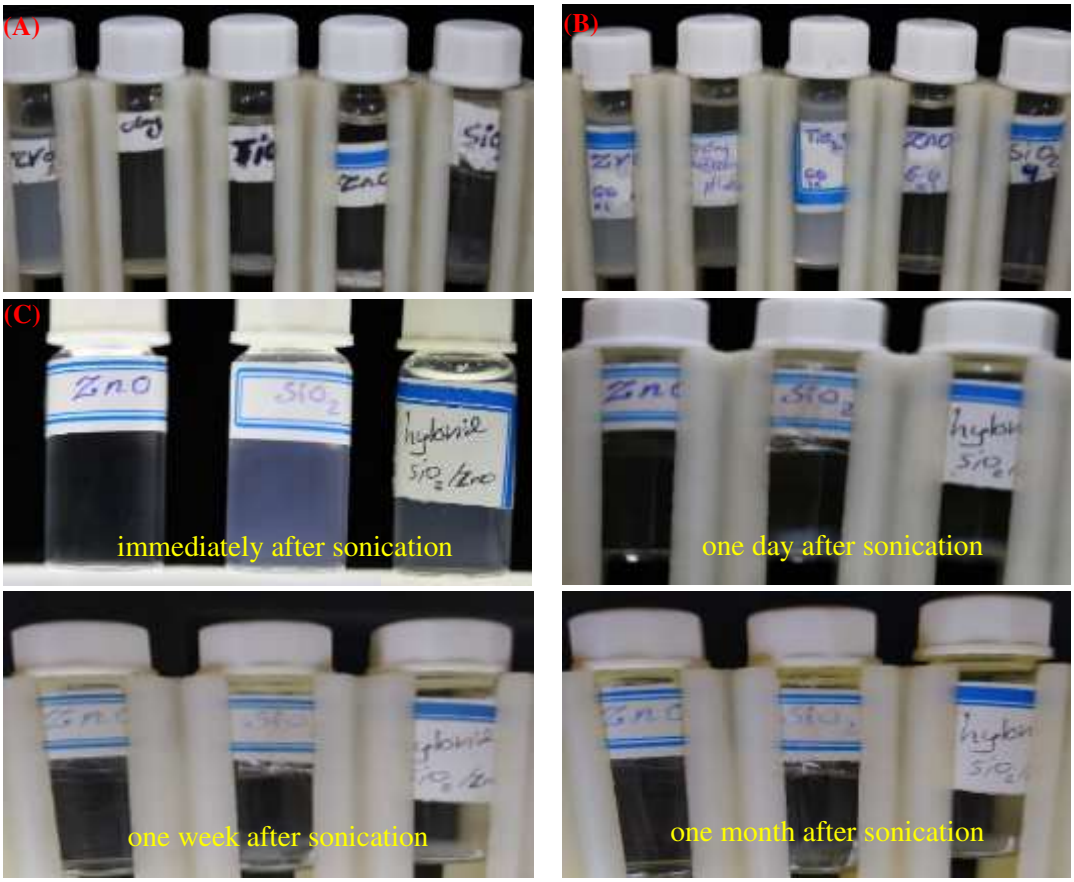

Figure 8. Evaluation of nanofluid stability in (A) basic environment of pH=11.7-12 and (B) acidic environment of pH=1.7-2 (base fluid: 20,000 ppm diluted formation water, FW2, NP: 0.05 wt%, guar gum polymer: 0.05 wt%), (C) ZnO and SiO_2, ZnO/SiO_2 nanofluid immediately after sonication, one day, one week, one month after sonication (base fluid: 80,000 ppm diluted formation water, FW8, NP: 0.05 wt%, guar gum polymer: 0.05 wt%, pH: 1.7-2, Temperature: 75°C)

The DLS diagrams of ZnO (0.05 wt%) with guar gam stabilizer (0.05 wt%) in seawater (80,000 ppm diluted formation water) are given in **Figure 9**. First, after the sonication sample, the DLS test was conducted. Then after one month under temperature of 75 °C, it was taken out from the oven and conducted the DLS again. Pertinent results to ZnO showed that the temperature did not bring any detrimental effect on the nanofluid stability and even reduced the diameter

of the suspended particles and made it more stable after a month (from 711 to 361.3 nm of Z-Average).

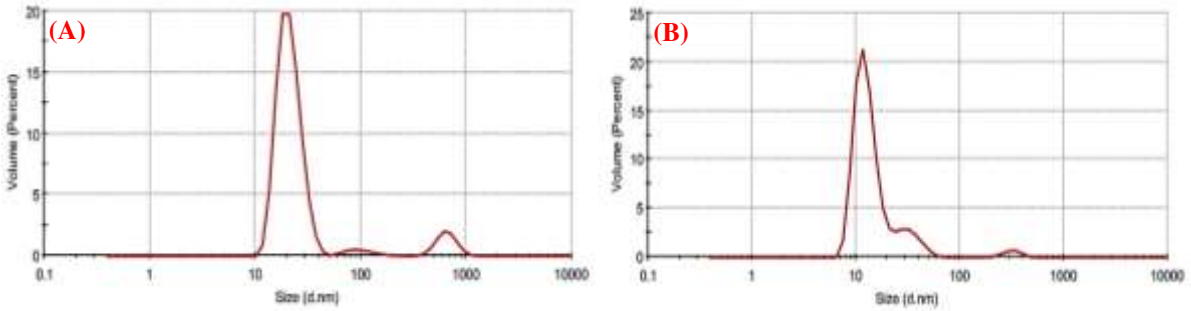

Figure 9. DLS results of ZnO nanofluid (A) immediately after sonication and (B) after a month keeping at temperature of 75 ℃ (base fluid: 40,572 ppm seawater, NP: 0.05 wt%, guar gum polymer: 0.05 wt%, pH: 1.7-2)

EOR Application Study of Seawater, Polymer Solution, Stabilized Nanofluid

After obtaining a stable nanofluid of zinc oxide NP stabilized by guar gum in seawater, the changes in the interfacial tension and carbonate surface contact angle were investigated to compare the results for the nanofluid, guar gum in seawater, and seawater, presented in **Table 8** and **Figure 10.** The guar gum concentration in the polymer solution and in the nanofluid was the same as the concentration of 0.05 wt%. The results showed a bit lower interfacial tension between the oil and nanofluid than that of the oil and polymer-seawater solution, probably because of the positive effect of association of nanoparticles with the polymer [69, 70]. Meanwhile, comparing the wettability alteration by the guar gum solution, seawater, ZnO nanofluid after one week showed that the nanofluid was capable to alter the wettability towards the carbonate rock hydrophilicity and the contact angle change of the carbonate rock from oil wet to water wet was much more than that of seawater and guar gum polymer solution.

Table 8. IFT reduction and contanct angle changes for seawater, polymer solution and ZnO nanofluid

Parameter	Seawater	Guar Gum Solution	Stabilized Nanofluid
Interfacial tension (mN/m)	20.47	19.30	18.74
Interfacial tension reduction (from seawater, mN/m)	0 (Ref)	(-1.17)	(-1.64)
Contact angle changes (degree)	26.6	88.77	113.68

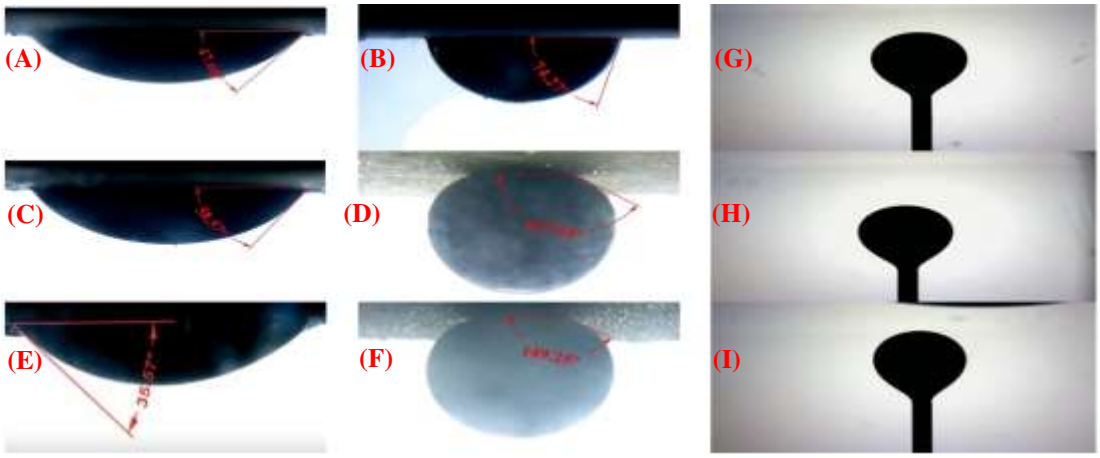

Figure 10. IFT reduction and contanct angle of seawater, polymer solution and ZnO nanofluid: (A) Seawater initial contact angle, (B) Seawater after 1 week contact angle, (C) Guar gam solution initial contact angle, (D) Guar gum solution after 1 week contact angle, (E) Nanofluid initial contact angle, (F) Nanofluid after 1 week contact angle, (G) Seawater IFT, (H) Guar gam solution IFT, (I) Nanofluid IFT

Figure 11 and **12** show the snapshots and obtained oil recovery factors for the chemical secondary and tertiary flooding tests in the glass micromodel. The ultimate oil recovery factors for the secondary flooding were 50.03, 65.90, 82.26% after injecting 2 PV of the seawater, guar gum in seawater, and polymer-stabilized ZnO in seawater, respectively. The breakthrough time occurred approximately 101, 138, 267 minutes after the injection began, and the amount of volume injected until the breakthrough were 0.38, 0.52, 1.00 PV, respectively. As can be observed, the results for the fluids injected into the micromodel in the secondary injection were significantly different. For instance, the secondary nanofluid injection enhanced the recovery factor by almost 1.6 times of the seawater injection. Additionally, the guar gum solution flooding without the presence of ZnO nanoparticles led to a recovery factor almost 1.3 times of the seawater injection. The nanofluid had a longer breakthrough time compared to that of SW and polymer solution. During the breakthrough, the pressure difference between the inlet and outlet of the micromodel was minimized. As a result, the breakthrough occurred later, the high-pressure injection phase swept the oil out of the pores, and thus a higher recovery factor was achieved. Meanwhile, the ultimate RF was 56.26% after the 2 PV tertiary flooding of stabilized-nanofluid which was enhanced the oil recovery by 6.27% compared to that of the seawater secondary injection (50.03%). The obtained results provided the high potential of ZnO nanofluid stabilized by guar gum polymer to increase the oil recovery.

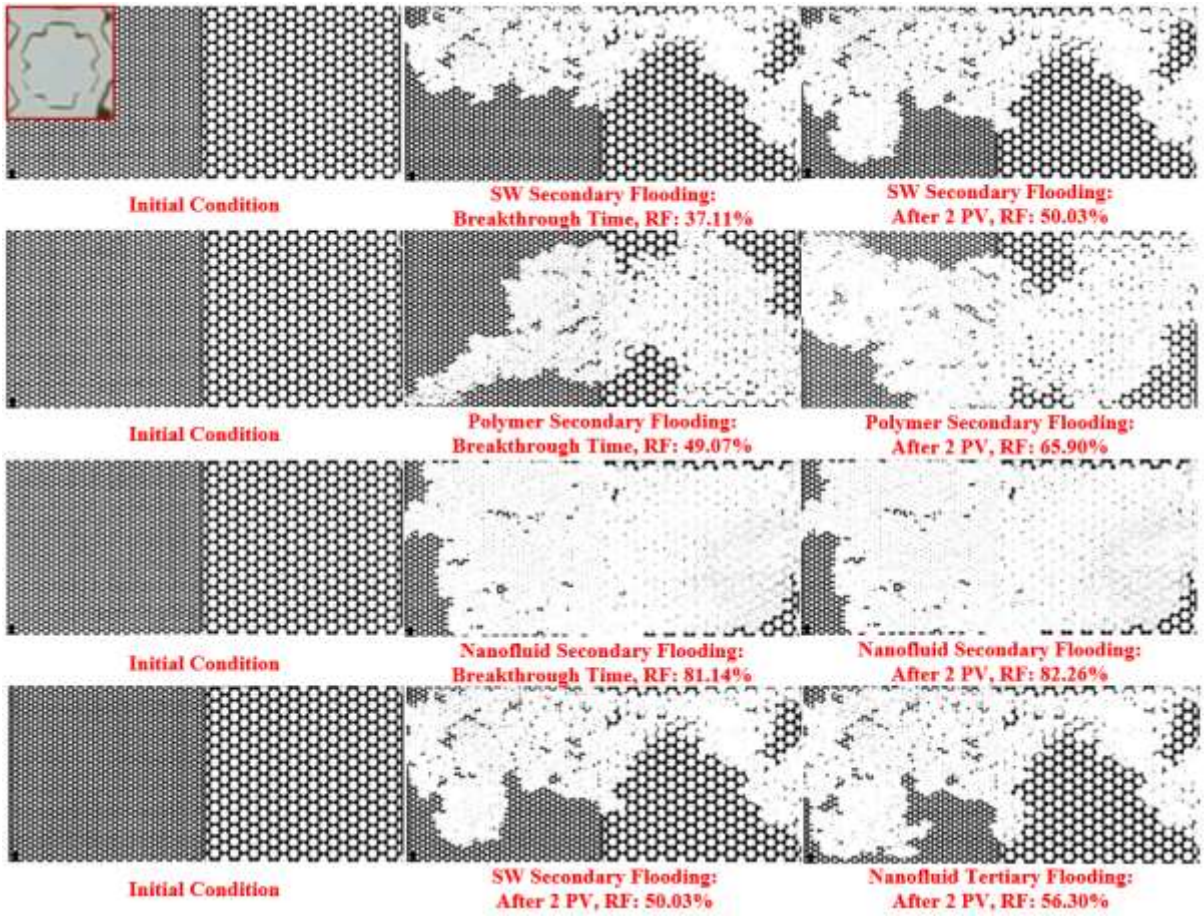

Figure 11. Snapshots of chemical secondary and tertiary flooding process
(ZnO concentration: 0.05 wt%, guar gum polymer concentration: 0.05 wt%, room temperature, complete oil-wet grain after aging in crude oil for 48 hours inserted)

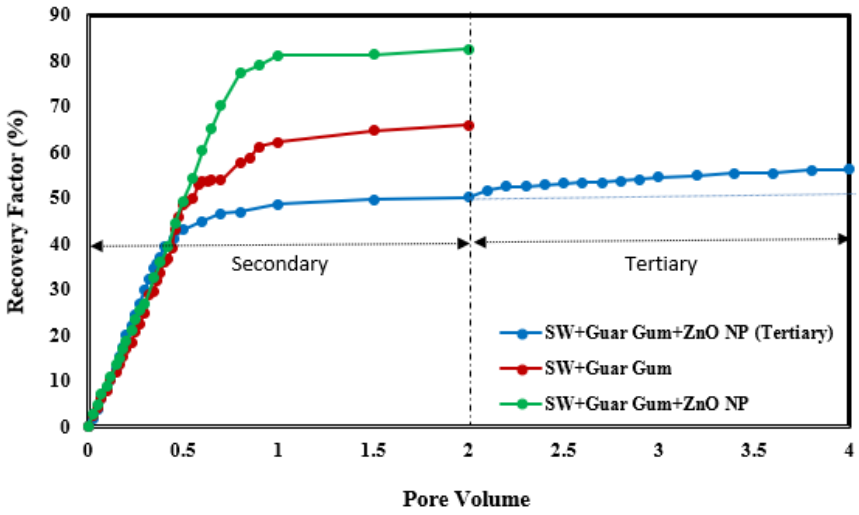

Figure 12. Oil recovery factor of chemical secondary and tertiary ZnO concentration: 0.05 wt%, guar gum polymer concentration: 0.05 wt%, room temperature

CONCLUSIONS

In this study, different nanoparticles were investigated to introduce a stable nanofluid for using in the oil recovery process at high temperature and high salinity and assess the synergistic effect of nanoparticles and stabilizer in seawater at pore scale through the glass micromodel. It was perceived that commingling ZnO and guar gum brought much more desirable results regarding the stability, wettability alteration, IFT reduction, and flooding performance compared to the other solutions. The most significant understandings are summarized as follow:

- The concentration of nanoparticles and the salinity of the base fluid had a proportional effect on the particle agglomeration and precipitation for the prepared nanofluids.
- Among the nanofluids of Al_2O_3, ZrO_2, TiO_2, Fe_2O_3, nanoclay and ZnO, Al_2O_3 nanoparticles in deionized water without stabilizer, Al_2O_3 and TiO_2 exhibited the highest and lowest stability, respectively.
- Compared to guar gum, PEG, PVP, TX100, CTAB, SDS stabilizers, the first one showed an excellent performance in stabilizing nanofluids.
- Among the nanofluids of Al_2O_3, SiO_2, ZrO_2, TiO_2, Fe_2O_3, nanoclay and ZnO, the two Al_2O_3 and Fe_2O_3 nanoparticles were more sensitive to salinity and left more agglomeration and precipitation.
- Experiments revealed that in general, SiO_2, ZrO_2, TiO_2, nanoclay, ZnO nanofluids were more stable at low pH values, hence, it could be inferred that the acidic medium boosted the nanofluid stability.
- Among the nanofluids of ZnO, Al_2O_3, SiO_2, ZrO_2, TiO_2, Fe_2O_3, nanoclay, only ZnO and SiO_2 nanofluids were able to maintain their stability at high salinity (80,000 ppm). Other nanofluids agglomerated by changing the base fluid to saline brine and precipitated at the bottom of the container.
- SiO_2 nanofluid exhibited a good stability at high salinity (80,000 ppm). However, increasing the temperature caused agglomeration, having a negative effect on the stability of the nanofluid.

- Increasing temperature not only did not cause zinc oxide to agglomerate, but also reduced the size of the suspended zinc oxide particles within the nanofluid. This reduction in the size simply led to nanofluid stability enhancement.
- Among ZnO, Al_2O_3, SiO_2, ZrO_2, TiO_2, Fe_2O_3, nanoclay nanofluids, only ZnO nanofluid remained stable at high temperature and salinity.
- Zinc oxide nanofluid showed stronger wettability alteration and a bit lower IFT reduction in comparison with the guar gum polymer solution and seawater.
- According to the secondary flooding tests of the micromodel, the nanofluid resulted in additional 16.36% and 32.23% in the oil recovery factor compared to that of guar gum polymer solution and seawater injection, respectively. This indicated an excellent potential of the mentioned nanofluid in the oil recovery processes.
- In the tertiary flooding test, the nanofluid led to an additional 6.27% increase in in the oil recovery factor compared to that of the secondary flooding by seawater.

DECLARATION OF INTEREST AND FUNDING STATEMENT

The authors declare that they have no known competing financial interests, funding resources from any supporters, and personal relationships that could have appeared to influence the work reported in "**Nanofluid Assisted-Chemical Oil Recovery Process at High Temperature and High Salinity Conditions: Nanofluid Stability, Interfacial Tension, Contact Angle, Microscale Experimental Investigation"**.

REFERENCES

[1]. Salem S.S., A mini review on green nanotechnology and its development in biological effects, *Archives of Microbiology*, 205, **2023**, https://doi.org/10.1007/s00203-023-03467-2.

[2]. Wahab A., A. Munir, M.H. Saleem, M. I. AbdulRaheem, H. Aziz, M. F. Bani Mfarrej, Gh. Abdi, Interactions of metal-based engineered nanoparticles with plants: An overview of the state of current knowledge, research progress, and prospects, *Journal of Plant Growth Regulation*, 235, **2023**, https://doi.org/10.1007/s00344-023-10972-7.

[3]. Lau H.C., M. Yu, Q.P. Nguyen, Nanotechnology for oilfield applications: challenges and impact, *Journal of Petroleum Science and Engineering*, 157, **2017**, 1160-1169, https://doi.org/10.1016/j.petrol.2017.07.062.

[4]. Joshi N., D.K. Pandey, B.G. Mistry, D.K. Singh (**2023**), Metal oxide nanoparticles: synthesis, properties, characterization, and applications. In: Singh, D.K., Singh, S., Singh, P. (eds) Nanomaterials. Springer, Singapore. https://doi.org/10.1007/978-981-19-7963-7_5

[5]. Haroun M., S. Al Hassan, A. Ansari, N. Al Kindy, N. Abou Sayed, B. Ali, S. Hemanta, Smart nano-EOR process for Abu Dhabi carbonate reservoirs, *Abu Dhabi International Petroleum Conference and Exhibition*, Abu Dhabi, UAE, **2012**, https://doi.org/10.2118/162386-MS.

[6]. Li S., L. Hendraningrat, O. Torsaeter. Improved oil recovery by hydrophilic silica nanoparticles suspension: Two phase flow experimental studies, *International Petroleum Technology Conference (IPTC)*, **2013**.

[7]. Esfandyari Bayat A., R. Junin, A. Samsuri, A. Piroozian, M. Hokmabadi, Impact of metal oxide Nanoparticles on enhanced oil recovery from limestone media at several temperatures, *Energy & Fuels*, 28, **2014**, https://doi.org/10.1021/ef5013616.

[8]. Hendraningrat L., O. Torsæter, Metal oxide-based nanoparticles: revealing their potential to enhance oil recovery in different wettability systems, *Applied Nanoscience*, 5, **2015**, https://doi.org/10.1007/s13204-014-0305-6.

[9]. Lee K. Ch., Z. A. bin Saipolbahri, H. Soleimani, H. M. Zaid, B. H. Guan, D. L. Chuan Ching, Effect of zinc oxide nanoparticle sizes on viscosity of nanofluid for application in enhanced oil recovery, *Journal of Nano Research*, 38, **2016**, https://doi.org/10.4028/www.scientific.net/JNanoR.38.36.

[10]. Yousefvand H.A., A. Jafari, Stability and flooding analysis of nanosilica/NaCl/HPAM/SDS solution for enhanced heavy oil recovery, *Journal of Petroleum Science and Engineering*, 162, **2018**, https://doi.org/10.1016/j.petrol.2017.09.078.

[11]. Rezk M.Y., N.K. Allam, Unveiling the synergistic effect of ZnO nanoparticles and surfactant colloids for enhanced oil recovery, *Colloid and Interface Science Communications*, 29, **2019**, https://doi.org/10.1016/j.colcom.2019.01.004.

[12]. Mahpishanian A. M., H. Shahverdi, M. Simjoo, M. R. Zaeri, Experimental investigation of nano silica on wettability alteration and enhanced oil recovery from carbonate reservoir using low salinity water, *Journal of Petroleum Research*, 30, **2021**, https://doi.org/10.22078/PR.2020.4187.2897.
[13]. Rashidi M., A. Kalantariasl, R. Saboori, A. Haghani, A. Keshavarz, Performance of environmentally friendly water-based calcium carbonate nanofluid as enhanced recovery agent for sandstone oil reservoirs, *Journal of Petroleum Science and Engineering*, 196, **2021**, https://doi.org/10.1016/j.petrol.2020.107644.
[14]. Bila A., O. Torsæter, Experimental investigation of polymer-coated silica nanoparticles for EOR under harsh reservoir conditions of high temperature and salinity, *Nanomaterials*, 11, **2021**, https://doi.org/10.3390/nano11030765.
[15]. Keykhosravi A., M.B. Vanani, and C. Aghayari, TiO_2 nanoparticle-induced xanthan gum polymer for EOR: Assessing the underlying mechanisms in oil-wet carbonates, *Journal of Petroleum Science and Engineering*, 204, **2021**, https://doi.org/10.1016/j.petrol.2021.108756.
[16]. Gu Z., Zh. Li, Zh. Xu, Ch. Zhang, Microscopic mechanical model analysis and visualization investigation of SiO_2 nanoparticle/HPAM polymer foam liquid film displacing heavy oil, *Langmuir*, 38, **2022**, https://pubs.acs.org/doi/10.1021/acs.langmuir.2c00817.
[17]. Xu L., X. Liu, Z. Liu, P. Li, H. Ding, H. Gong, M. Dong, Extensional rheology of hydrophobically associating polyacrylamide solution used in chemical flooding: Effects of temperature, NaCl and surfactant, *Chemical Engineering Science*, 273, **2023**, https://doi.org/10.1016/j.ces.2023.118644.
[18]. Pu J.Y., K. P. Johnston, P.K. Wu, M. Ahmad, M. L. Luo, N. Zhang, J. T. He, Facile synthesis of chromium chloride/poly(methyl methacrylate) core/shell nanocapsules by inverse miniemulsion evaporation method and application as delayed crosslinker in secondary oil recovery, *Petroleum Science*, 20, **2023**, https://doi.org/10.1016/j.petsci.2022.09.031.
[19]. Almahfood M., B. Bai, The synergistic effects of nanoparticle-surfactant nanofluids in EOR applications, *Journal of Petroleum Science and Engineering*, 171, **2018**, https://doi.org/10.1016/j.petrol.2018.07.030.
[20]. Karakosta O., A. C. Mitropoulos, G. Z. Kyzas, A review in nanopolymers for drilling fluids applications, *Journal of Molecular Structure*, 1227, **2021**, https://doi.org/10.1016/j.molstruc.2020.129702.
[21]. Moghadam T.F., S. Azizian, Effect of ZnO nanoparticles on the interfacial behavior of anionic surfactant at liquid/liquid interfaces, *Colloids and Surfaces A: Physicochemical and Engineering Aspects*, 457, **2014,** https://doi.org/10.1016/j.colsurfa.2014.06.009.
[22]. Fedele L., L. Colla, S. Bobbo, S. Barison, F. Agresti, Experimental stability analysis of different water-based nanofluids, *Nanoscale Research Letters*, 6, **2011**, https://doi.org/10.1186/1556-276X-6-300.
[23]. Wusiman K., H. Jeong, K. Tulugan, H. Afrianto, H. Chung, Thermal performance of multi-walled carbon nanotubes (MWCNTs) in aqueous suspensions with surfactants SDBS and SDS, *International Communications in Heat and Mass Transfer*, 41, **2013**, https://doi.org/10.1016/j.icheatmasstransfer.2012.12.002.
[24]. López-Miranda A., A. López-Valdivieso, and G. Viramontes-Gamboa, Silver nanoparticles synthesis in aqueous solutions using sulfite as reducing agent and sodium dodecyl sulfate as stabilizer, *Journal of Nanoparticle Research*, 14, **2012,** https://doi.org/10.1007/s11051-012-1101-4.
[25]. Xian-Ju W., L. Hai, L. Xin-Fang, W. Zhou-Fei, L. Fang, Stability of TiO_2 and Al_2O_3 nanofluids, *Chinese Physics Letters*, 28, **2011**, https://doi.org/10.1088/0256-307X/28/8/086601.
[26]. Hwang Y., J. K. Lee, J. K. Lee, Y. M. Jeong, S. Cheong, Y. Ch. Ahn, S. H. Kim, Production and dispersion stability of nanoparticles in nanofluids, *Powder Technology*, 186, **2008,** https://doi.org/10.1016/j.powtec.2007.11.020.
[27]. Zhang X., H. Gu, M. Fujii, Effective thermal conductivity and thermal diffusivity of nanofluids containing spherical and cylindrical nanoparticles, *Experimental Thermal and Fluid Science*, 31, **2007,** https://doi.org/10.1016/j.expthermflusci.2006.06.009.
[28]. Hwang, Y., Y.C. Ahn, H.S. Shin, C.G. Lee, G.T. Kim, H.S. Park, J.K. Lee, Investigation on characteristics of thermal conductivity enhancement of nanofluids, *Current Applied Physics*, 6, **2006,** https://doi.org/10.1016/j.cap.2005.07.021.
[29]. Tadros T., Th. Tadros, P. Izquierdo, J. Esquena, C. Solans, Formation and stability of nano-emulsions, *Advances in Colloid and Interface Science*, 108, **2004,** https://doi.org/10.1016/j.cis.2003.10.023.
[30]. Jiang, L., L. Gao, J. Sun, Production of aqueous colloidal dispersions of carbon nanotubes, *Journal of Colloid and Interface Science*, 260, **2003,** https://doi.org/10.1016/S0021-9797(02)00176-5.
[31]. Khairul M., K. Shah, E. Doroodchi, R.Azizian, B. Moghtaderi, Effects of surfactant on stability and thermo-physical properties of metal oxide nanofluids, *International Journal of Heat and Mass Transfer*, 98, **2016**, https://doi.org/10.1016/j.ijheatmasstransfer.2016.03.079.
[32]. LotfizadehDehkordi, B., S. N. Kazi, M. Hamdi, A. Ghadimi, E. Sadeghinezhad, H. S. C. Metselaar, Investigation of viscosity and thermal conductivity of alumina nanofluids with addition of SDBS, *Heat and Mass Transfer Journal*, 49, **2013**, https://doi.org/10.1007/s00231-013-1153-8.
[33]. Wang Z., A. Lam, E. Acosta, Suspensions of iron oxide nanoparticles stabilized by anionic surfactants, *Journal of Surfactants and Detergents*, 16, **2013**, https://doi.org/10.1007/s11743-012-1425-1.

[34]. Bac L., W.H. Gu, J.C. Kim, B.K. Kim, J.S. Kim, Characterization and stability of silver nanoparticles in aqueous solutions, *Journal of Korean Powder Metallurgy Institute*, 19, **2012**, https://doi.org/10.4150/KPMI.2012.19.1.055.
[35]. Cui S., B. Lin, M. Fan, X. Shen, Interaction mechanism between Fe_3O_4 nanoparticles and sodium 2-dodecylbenzenesulfonate, *Current Nanoscience*, 7, **2011**, https://doi.org/10.2174/157341311795542417.
[36]. Wei X., H. Zhu, T. Kong, L. Wang, Synthesis and thermal conductivity of Cu_2O nanofluids, *International Journal of Heat and Mass Transfer*, 52, **2009**, https://doi.org/10.1016/j.ijheatmasstransfer.2009.03.073.
[37]. Wang XJ., X. Li, S. Yang, Influence of pH and SDBS on the stability and thermal conductivity of nanofluids, *Energy & Fuels*, 23, **2009**, https://doi.org/10.1021/ef800865a.
[38]. Li X., D.S. Zhu, X.J. Wang, N. Wang, J.W. Gao, H. Li, Thermal conductivity enhancement dependent pH and chemical surfactant for Cu-H_2O nanofluids, *Thermochimica Acta*, 469, **2008**, https://doi.org/10.1016/j.tca.2008.01.008.
[39]. Song X., N. Jiang, Y. Li, D. Xu, G. Qiu, Synthesis of CeO_2-coated SiO_2 nanoparticle and dispersion stability of its suspension, *Materials Chemistry and Physics*, 110, **2008**, https://doi.org/10.1016/j.matchemphys.2008.01.042.
[40]. Gbadamosi A.O., R. Junin, M. A. Manan, N. Yekeen, A. Agi, J. O. Oseh, Recent advances and prospects in polymeric nanofluids application for enhanced oil recovery, *Journal of Industrial and Engineering Chemistry*, 66, **2018**, https://doi.org/10.1016/j.jiec.2018.05.020.
[41]. Pantzali M., A. Mouza, S. Paras, Investigating the efficacy of nanofluids as coolants in plate heat exchangers (PHE), *Chemical Engineering Science*, 64, **2009**, https://doi.org/10.1016/j.ces.2009.04.004.
[42]. Sun Q., Zh. Li, S. Li, L. Jiang, J. Wang, Peng Wang, Utilization of surfactant-stabilized foam for enhanced oil recovery by adding nanoparticles, *Energy & Fuels*, 28, **2014**, https://doi.org/10.1021/ef402453b.
[43]. Sobhan M.A., M.J. Withford, E.M. Goldys, Enhanced stability of gold colloids produced by femtosecond laser synthesis in aqueous solution of CTAB, *Langmuir*, 26, **2010**, https://doi.org/10.1021/la903088e.
[44]. Rahevar S., A. Kakati, G. Kumar, J. Sangwai, M. Myers, A. Al-Yaseri, Controlled salinity water flooding and zeta potential: Insight into a novel enhanced oil recovery mechanism, *Energy Reports*, 9, **2023**, https://doi.org/10.1016/j.egyr.2023.01.088.
[45]. Sui Z., X. Chen, L.Y. Wang, L.M. Xu, W.C. Zhuang, Y.C. Chai, C.J. Yang, Capping effect of CTAB on positively charged Ag nanoparticles, *Physica E: Low-dimensional Systems and Nanostructures*, 33, **2006**, https://doi.org/10.1016/j.physe.2006.03.151.
[46]. Assael M., I. N. Metaxa, J. Arvanitidis, D. Christofilos, C. Lioutas, Thermal conductivity enhancement in aqueous suspensions of carbon multi-walled and double-walled nanotubes in the presence of two different dispersants, *International Journal of Thermophysics*, 26, **2005**, https://doi.org/10.1007/s10765-005-5569-3.
[47]. Madni I., Ch. Y. Hwang, S. D. Park, Y. H. Choa, H. Taik Kim, Mixed surfactant system for stable suspension of multiwalled carbon nanotubes, *Colloids and Surfaces A: Physicochemical and Engineering Aspects*, 358, **2010**, https://doi.org/10.1016/j.colsurfa.2010.01.030.
[48]. Tejamaya M., I. Römer, R. C. Merrifield, J. R. Lead, Stability of citrate, PVP, and PEG coated silver nanoparticles in ecotoxicology media, *Environmental Science & Technology*, 46, **2012**, https://doi.org/10.1021/es2038596.
[49]. Ma T., Y. Kong, H. Liu, X. Xu, Q. Yue, B. Gao, Y. Gao, One-step synthesis of Enteromorpha graphene aerogel modified by hydrophilic polyethylene glycol achieving high evaporation efficiency and pollutant tolerance, *Journal of Colloid and Interface Science*, 633, **2023**, https://doi.org/10.1016/j.jcis.2022.11.145.
[50]. McFarlane N.L., N. J. Wagner, E. W. Kaler, M. L. Lynch, Poly(ethylene oxide)(PEO) and poly(vinyl pyrolidone)(PVP) induce different changes in the colloid stability of nanoparticles, *Langmuir*, 26, **2010**, https://doi.org/10.1021/la101907s.
[51]. Walleck C.J., Development of steady-state, parallel-plate thermal conductivity apparatus for poly-nanofluids and comparative measurements with transient HWTC apparatus, **2009**, *Northern Illinois University*.
[52]. Zhu H., C. Zhang, Y. Tang, J. Wang, B. Ren, Y. Yin, Preparation and thermal conductivity of suspensions of graphite nanoparticles, *Carbon*, 45, **2007**, https://doi.org/10.1016/j.carbon.2006.07.005.
[53]. Williams D.N., K. A. Gold, T. R. P. Holoman, Sh.H. Ehrman, O. C. Wilson Jr, Surface modification of magnetic nanoparticles using gum Arabic, *Journal of Nanoparticle Research*, 8, **2006**, https://doi.org/10.1007/s11051-006-9084-7.
[54]. Rashmi W., A.F. Ismail, I. Sopyan, A.T. Jameel, F. Yusof, M. Khalid, N.M. Mubarak, Stability and thermal conductivity enhancement of carbon nanotube nanofluid using gum Arabic, *Journal of Experimental Nanoscience*, 6, **2011**, https://doi.org/10.1080/17458080.2010.487229.
[55]. Tiraferri A., K. Loon Chen, R. Sethi, M. Elimelech, Reduced aggregation and sedimentation of zero-valent iron nanoparticles in the presence of guar gum, *Journal of Colloid and Interface Science*, 324, **2008**, https://doi.org/10.1016/j.jcis.2008.04.064.
[56]. Tiraferri A., R. Sethi, Enhanced transport of zerovalent iron nanoparticles in saturated porous media by guar gum, *Journal of Nanoparticle Research*, 11, **2009**, https://doi.org/10.1007/s11051-008-9405-0.

[57]. Zhu H. T., Y. S. Lin, Y. S. Yin, A novel one-step chemical method for preparation of copper nanofluids, *Journal of Colloid and Interface Science*, 277, **2004**, https://doi.org/10.1016/j.jcis.2004.04.026.
[58]. Kumar S., S. Kumar, B. Kumar, R. Sehgal, M. F. Wani, D. Kumar, M. D. Sharma, V. Singh, R. Sehgal, V. Kumar (**2023**). Advantages and disadvantages of metal nanoparticles. In: Tiwari, S.K., Kumar, V., Thomas, S. (eds) Nanoparticles Reinforced Metal Nanocomposites, Springer, Singapore, https://doi.org/10.1007/978-981-19-9729-7_7.
[59]. Wu D., H. Zhu, L. Wang, L. Liu, Critical issues in nanofluids preparation, characterization and thermal conductivity, *Current Nanoscience*, 5, **2009**, https://doi.org/10.2174/157341309787314548.
[60]. Wang X. Q., A.S. Mujumdar, Heat transfer characteristics of nanofluids: a review, *International Journal of Thermal Sciences*, 46, 2007, https://doi.org/10.1016/j.ijthermalsci.2006.06.010.
[61]. Murshed S., K. Leong, C. Yang, Investigations of thermal conductivity and viscosity of nanofluids, *International Journal of Thermal Sciences*, 47, **2008**, https://doi.org/10.1016/j.ijthermalsci.2007.05.004.
[62]. Al-Anssari S., S. Al-Anssari, Sh. Wang, A. Barifcani, M. Lebedev, S. Iglauer, Effect of temperature and SiO_2 nanoparticle size on wettability alteration of oil-wet calcite, *Fuel*, 206, **2017**, https://doi.org/10.1016/j.fuel.2017.05.077.
[63]. Adil M., H. M. Zaid, L. Kean Chuan, N. R. Ahmad Latiff, Effect of dispersion stability on electrorheology of water-based ZnO nanofluids, *Energy & Fuels*, 30, **2016**, https://doi.org/10.1021/acs.energyfuels.6b01116.
[64]. Nourafkan E., M. Asachi, Zh. Hu, H. Gao, D. Wen, Synthesis of stable nanoparticles at harsh environment using the synergistic effect of surfactants blend, *Journal of Industrial and Engineering Chemistry*, 64, **2018**, https://doi.org/10.1016/j.jiec.2018.04.002.
[65]. Metin C.O., L. W. Lake, C. R. Miranda, Q.P. Nguyen, Stability of aqueous silica nanoparticle dispersions, *Journal of Nanoparticle Research*, 13, **2011**, https://doi.org/10.1007/s11051-010-0085-1.
[66]. Saleh N., H. J. Kim, T. Phenrat, K. Matyjaszewski, R. D. Tilton, G. V. Lowry, Ionic strength and composition affect the mobility of surface-modified Fe0 nanoparticles in water-saturated sand columns, *Environmental Science & Technology*, 42, **2008**, https://doi.org/10.1021/es071936b.
[67]. He Y.T., J. Wan, T. Tokunaga, Kinetic stability of hematite nanoparticles: the effect of particle sizes, *Journal of Nanoparticle Research*, 10, **2008**, https://doi.org/10.1007/s11051-007-9255-1.
[68]. Naito M., T. Yokoyama, K. Hosokawa, K, Nogi (**2021**), Nanoparticle Technology Handbook (third edition), https://doi.org/10.1016/C2017-0-01011-X.
[69]. Dong, L., D. Johnson, Surface tension of charge-stabilized colloidal suspensions at the water− air interface, *Langmuir*, 19, **2003**, https://doi.org/10.1021/la035128j.
[70]. Ravera, F., E. Santini, G. Loglio, M. Ferrari, L. Liggieri, Effect of nanoparticles on the interfacial properties of liquid/liquid and liquid/air surface layers, *The Journal of Physical Chemistry B*, 110, **2006**, https://doi.org/10.1021/jp0636468.